Int. J. Solids Structures Vol. 15, pp. 303–318

0020-7683/79/0401-0303/$02.00/0

PROPAGATION OF TRANSIENT WAVES IN ELASTIC LAMINATED COMPOSITES

HUGH D. MCNIVEN

Professor of Engineering Science, University of California, Berkeley, CA 94720, U.S.A.

and

YALCIN MENGI†

Associate Professor of Engineering, The Middle East Technical University, Ankara, Turkey

(*Received* 2 *August* 1978; *received for publication* 5 *September* 1978)

Abstract—The paper is devoted to the appraisal of a model material which can be used to replace one constructed of alternate plane layers. The material is homogeneous, anisotropically elastic and is dispersive. The purpose of the model is to study the dynamic response of masonry walls. The equations governing the model consist of constitutive equations and equations of linear momentum. The theory is constructed using the theory of mixtures and dispersion is accommodated by means of elastodynamic operators introduced into the equations of linear momentum. The theory contains nineteen constants. The derivation of the governing equations and equations relating the model constants to those of the prototype are presented in earlier papers.

In this paper we appraise the model by comparing the responses predicted by the model for a transient input with those observed experimentally. Experimental data allow us to make comparisons for the behavior of dilatational waves travelling both parallel and perpendicular to the layers in both plates and semi-infinite bodies. Where possible, comparison is also made with responses predicted by the exact theory. Responses in the model are found using the method of characteristics. Comparison is exhibited in a number of figures and shows that the responses predicted by the theory are quite accurate. The accuracy is not restricted to early arrival times but extends to behavior far behind the head of the pulse.

1. INTRODUCTION

This paper is the third in a series of three devoted to the general problem of predicting the elastic response of masonry walls to dynamic inputs. The wall is recognized as consisting of two materials, or phases, and is predominantly a layered array. The method for predicting its dynamic behavior is to replace the wall by a model material that is homogeneous, elastic and dispersive. In the series we derive equations governing the dynamic behavior of the material, introduce ways of finding the model constants that appear in the theory, and assess the model by comparing dynamic responses predicted by its theory with known response data both theoretical and experimental.

In the first paper[1] a general theory is developed for all two phase materials for which the phases display a periodic array. The equations governing the model are of two kinds, constitutive equations and equations of linear momentum. The dispersive properties of the model are reflected through eastodynamic operators that appear in the equations of linear momentum. The theory was derived using the theory of mixtures, for two principal reasons. Firstly, the approximate theory based on this approach has governing equations simple enough to be employed in practical engineering problems. Secondly, the mixture approach makes it possible to express the governing equations of all two phase composites in a common form. Hence the approximate theory for a complicated two phase composite can be improved by modifying the constants or operators appearing in the theory while keeping the general form of the governing equations unchanged.

In the second paper[2] the general theory is adapted to a specific geometry; a two phase material consisting of alternate plane layers of different isotropically elastic properties. The adaption consists first of reducing the number of independent constants in the stiffness matrix according to the symmetries introduced. With a specific geometry the form of the elastodynamic operator is developed using a micro model analysis. Next, an approximate form for

†Visiting Assistant Research Engineer, University of California, Berkeley, CA 94720, U.S.A.

the operators is obtained by expanding them in power series and retaining the first three terms. The form of the theory is complete when these operators are introduced into the equations of linear momentum.

The theory contains nineteen constants which have to be related to the mechanical properties of each of the two layers in the prototype. The logic behind this final step in constructing the model is to develop the relationships in such a way that the model and prototype will behave as much alike as possible in their dynamic behaviors. The best set of constants would undoubtedly be obtained by matching specific dynamic behaviors, as extensively as possible, using a rational procedure such as system identification. With nineteen parameters this procedure would be formidable so we choose instead what we consider to be the simplest method of establishing the nineteen independent equations. The equations are derived partly using micro model analysis and partly by matching cut-off phase velocities and frequencies and asymptotic phase velocities of spectra representing the theoretical behavior of infinite trains of waves propagating both parallel and perpendicular to the layers. With the nineteen equations for evaluating the constants, the theory is complete.

The second paper ends with a preliminary assessment of the theory made by comparing spectral lines derived from it, representing the relationships between phase velocity and wave length or frequency and wave length, with comparable lines derived both from other theories and from experiments.

In this paper we subject the theory to what seems to us to be the most demanding test. That is comparison of the responses predicted by the theory with experimental transient responses. We are fortunate in having available excellent experimental data for transient waves propagating both parallel and perpendicular to the layers.

The transient responses predicted by the theory are obtained using the method of characteristics. This method is chosen, first because the governing equations are hyperbolic, and secondly because symmetry reduces the number of independent variables to time and one space variable. Where it seems appropriate we also make comparisons with responses predicted by the exact theory and by another approximate theory.

The theory for the model we have developed is, we think, simple for such a problem, the method of finding the constants is simple, so we are gratified to find such extensive matching between the responses due to the theory and to experiments. The matching is displayed in a number of figures. Not only do the profiles match for early times after the arrival of the first disturbance at a number of stations in the material, they also match well at distances remote from the head of the pulse.

2. BASIC EQUATIONS

For completeness we start our study by reviewing the governing equations of the approximate theory developed in[2] for a layered composite. The composite consists of two perfectly bonded alternating layers of thicknesses $2h_1$ and $2h_2$. We assume that the layers are made of different isotropically elastic materials with the properties $(\mu_\alpha, \lambda_\alpha, \rho_\alpha{}^R)$ $(\alpha = 1, 2)$, where $(\mu_\alpha, \lambda_\alpha)$ and $\rho_\alpha{}^R$ are Lamé's constants and the mass density, respectively, of the layer. We refer the composite to a Cartesian coordinate system (x_1, x_2, x_3) in which the x_2 axis is perpendicular to the plane of layering. The governing equations of the two mode approximate theory developed in[2] are composed of linear momentum and constitutive equations. The equations of linear momentum are

$$\begin{aligned} \frac{\partial \sigma_{ji}^1}{\partial x_j} + \rho_1 F_i^1 + K_{ij}(u_j^2 - u_j^1) &= m_{ij}^1 \dot{v}_j^1 - q_{ij} \dot{v}_j^2 \\ \frac{\partial \sigma_{ji}^2}{\partial x_j} + \rho_2 F_i^2 + K_{ij}(u_j^1 - u_j^2) &= -q_{ij} \dot{v}_j^1 + m_{ij}^2 \dot{v}_j^2. \end{aligned} \tag{2.1}$$

The first and second of eqns (2.1) are written for the first and second constituents, respectively, of the composite material. In these equations subscripts take the values 1, 2 and 3, and any repeated index implies summation over the range of that index. Throughout the paper Greek indices $(\alpha, \beta, \ldots)$ will be used only for distinguishing quantities pertaining to two different

phases. Summation over the Greek indices will be indicated by using a summation symbol. The terms appearing in eqns (2.1) are defined by $\rho_\alpha = n_\alpha \rho_\alpha^R$, partial masses for phases, measured per unit volume of composite; $n_\alpha = h_\alpha/\Delta$, the volume fraction of the α phase with the property $\sum_{\alpha=1}^{2} n_\alpha = 1$, where $\Delta = \sum_{\alpha=1}^{2} h_\alpha$; v_i^α, average velocity components for phases; u_i^α, average displacement components for phases; σ_{ij}^α, partial stress components for a phase, measured per unit area of composite; and $\rho_\alpha F_i^\alpha$, body force components for a phase, measured per unit volume of composite. The dot denotes partial differentiation with respect to time and

$$(K_{ij}) = \begin{bmatrix} K_1 & 0 & 0 \\ 0 & K_2 & 0 \\ 0 & 0 & K_1 \end{bmatrix}; \quad (q_{ij}) = \begin{bmatrix} q_1 & 0 & 0 \\ 0 & q_2 & 0 \\ 0 & 0 & q_1 \end{bmatrix} (m_{ij}^\alpha) = \begin{bmatrix} (\rho_\alpha + q_1) & 0 & 0 \\ 0 & (\rho_\alpha + q_2) & 0 \\ 0 & 0 & (\rho_\alpha + q_1) \end{bmatrix} \tag{2.2}$$

where K_α and q_α are constants. In[2] a simple procedure for evaluation of the constants appearing in the approximate theory is presented. In that procedure the K_α are determined using micro model analysis, while the q_α are found so that the approximate and exact cut-off frequencies match. They are found to be

$$K_1 = \frac{3r_1 r_2}{\Delta^2 r}; \qquad K_2 = \frac{3E_1 E_2}{\Delta^2 E}$$
$$q_\alpha = \frac{1}{\rho}\left(\frac{\rho K_\alpha}{\bar{\omega}_\alpha^2} - \rho_1 \rho_2\right) \tag{2.3}$$

where

$$r_\alpha = \frac{\mu_\alpha}{n_\alpha}; \qquad r = \sum_{\alpha=1}^{2} r_\alpha$$
$$E_\alpha = \frac{2\mu_\alpha + \lambda_\alpha}{n_\alpha}; \qquad E = \sum_{\alpha=1}^{2} E_\alpha \tag{2.4}$$
$$\rho = \sum_{\alpha=1}^{2} \rho_\alpha.$$

The $\bar{\omega}_\alpha$ denote the exact cut-off frequencies for principal waves propagating parallel and perpendicular to layering.

In the absence of thermal effects, the constitutive equations are

$$\begin{Bmatrix} \boldsymbol{\sigma}^1 \\ \boldsymbol{\sigma}^2 \end{Bmatrix} = \begin{bmatrix} \mathbf{C}^{11} & \mathbf{C}^{12} \\ \mathbf{C}^{21} & \mathbf{C}^{22} \end{bmatrix} \begin{Bmatrix} \mathbf{e}^1 \\ \mathbf{e}^2 \end{Bmatrix}. \tag{2.5}$$

In eqns (2.5) $\boldsymbol{\sigma}^\alpha$ and $\mathbf{e}^\alpha$ are vector representations of the stress and strain tensors:

$$\boldsymbol{\sigma}^\alpha = (\sigma_{11}^\alpha, \sigma_{22}^\alpha, \sigma_{33}^\alpha, \sigma_{12}^\alpha, \sigma_{13}^\alpha, \sigma_{23}^\alpha)$$
$$\mathbf{e}^\alpha = (e_{11}^\alpha, e_{22}^\alpha, e_{33}^\alpha, 2e_{12}^\alpha, 2e_{13}^\alpha, 2e_{23}^\alpha), \tag{2.6}$$

where the strain components for the α phase e_{ij}^α are defined by

$$e_{ij}^\alpha = \frac{1}{2}\left(\frac{\partial u_i^\alpha}{\partial x_j} + \frac{\partial u_j^\alpha}{\partial x_i}\right); \tag{2.7}$$

the $\mathbf{C}^{\alpha\beta}$ are 6×6 material coefficient matrices. In[1], using thermodynamic analysis it is shown that for a general two phase composite the matrices $\mathbf{C}^{11}$ and $\mathbf{C}^{22}$ are both symmetric and $\mathbf{C}^{21} = (\mathbf{C}^{12})^T$. For a layered composite having hexagonal symmetry with x_2 the axis of symmetry, the $\mathbf{C}^{\alpha\beta}$ are given by

$$\mathbf{C}^{\alpha\beta} = \begin{bmatrix} C_{11}^{\alpha\beta} & C_{12}^{\alpha\beta} & C_{13}^{\alpha\beta} & 0 & 0 & 0 \\ C_{12}^{\alpha\beta} & C_{22}^{\alpha\beta} & C_{12}^{\alpha\beta} & 0 & 0 & 0 \\ C_{13}^{\alpha\beta} & C_{12}^{\alpha\beta} & C_{11}^{\alpha\beta} & 0 & 0 & 0 \\ 0 & 0 & 0 & C_{44}^{\alpha\beta} & 0 & 0 \\ 0 & 0 & 0 & 0 & C_{55}^{\alpha\beta} & 0 \\ 0 & 0 & 0 & 0 & 0 & C_{44}^{\alpha\beta} \end{bmatrix} \text{(for } \alpha = \beta\text{)}, \tag{2.8}$$

where $C_{55}^{\alpha\beta} = (1/2)\,(C_{11}^{\alpha\beta} - C_{13}^{\alpha\beta})$, and

$$\mathbf{C}^{12} = \begin{bmatrix} C_{11}^{12} & C_{12}^{12} & C_{11}^{12} & 0 & 0 & 0 \\ C_{21}^{12} & C_{22}^{12} & C_{21}^{12} & 0 & 0 & 0 \\ C_{11}^{12} & C_{12}^{12} & C_{11}^{12} & 0 & 0 & 0 \\ 0 & 0 & 0 & C_{44}^{12} & 0 & 0 \\ 0 & 0 & 0 & 0 & 0 & 0 \\ 0 & 0 & 0 & 0 & 0 & C_{44}^{12} \end{bmatrix}. \tag{2.9}$$

In [2] a procedure is presented for evaluation of fifteen independent constants appearing in eqns. (2.8) and (2.9). The method uses both micro model analysis and matching the spectra predicted by the exact and approximate theories. In the present study we are concerned only with dilatational transient waves propagating parallel and perpendicular to the layering. Accordingly our analysis involves only the constants $C_{11}^{\alpha\beta}$ and $C_{22}^{\alpha\beta}$ and we present only those equations from which these constants can be found. The $C_{11}^{\alpha\beta}$ are found using the equations,

$$C_{11}^{11} = n_1{}^2 E_1 - \frac{\lambda_1{}^2}{E}; \qquad C_{11}^{22} = n_2{}^2 E_2 - \frac{\lambda_2{}^2}{E}; \qquad C_{11}^{12} = C_{11}^{21} = \frac{\lambda_1 \lambda_2}{E}, \tag{2.10}$$

and the $C_{22}^{\alpha\beta}$ are derived from the set of equations

$$\begin{aligned} C_{22}^{11} + C_{22}^{22} + 2C_{22}^{12} &= \frac{E_1 E_2}{E} \\ C_{22}^{11} C_{22}^{22} - C_{22}^{12} C_{22}^{12} &= 0 \\ \rho_1 C_{22}^{22} + \rho_2 C_{22}^{11} &= (\rho_1 \rho_2 + \rho q_2)\, c_\infty^2 - q_2 \frac{E_1 E_2}{E}, \end{aligned} \tag{2.11}$$

where

$$c_\infty = \frac{\sqrt{\left(\frac{E_1}{\rho_1}\right)}\sqrt{\left(\frac{E_2}{\rho_2}\right)}}{\sqrt{\left(\frac{E_1}{\rho_1}\right)} + \sqrt{\left(\frac{E_2}{\rho_2}\right)}}. \tag{2.12}$$

3. FORMULATION OF THE PROBLEMS

In this study, we compare the transient responses predicted by the theory developed in [2] with those obtained experimentally and with those from the theory of elasticity. The comparison is made for dilatational waves propagating parallel and perpendicular to the layering since experimental data and the data derived from the equations of elasticity are available for these particular waves [3–5].

The problems that we study are those dictated by the experiments from which we have data for transient responses. They involve either layered half spaces or layered plates; and we study the cases where the layers are parallel to the surface of the half space or one surface of the plate, and the cases where the layers are normal to these surfaces. The time dependent normal pressure is applied to these surfaces so that for the first cases dilatational waves are generated normal to the layers, and for the second cases parallel to them (see Figs. 3–9). We assume that the composite slabs or half spaces are initially at rest before the normal pressure is applied.

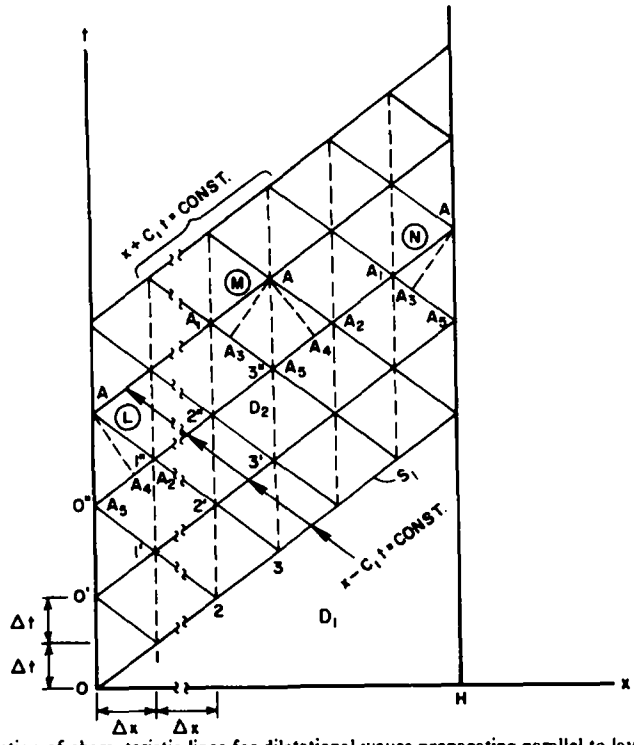

Fig. 1. Description of characteristic lines for dilatational waves propagating parallel to layering in a layered composite slab of thickness H.

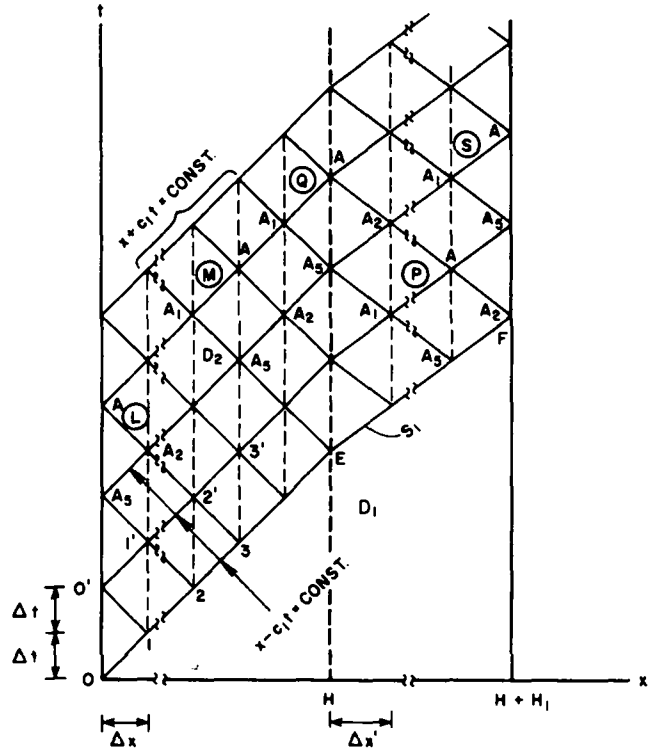

Fig. 2. Description of characteristic lines for dilatational waves propagating perpendicular to layering in a layered composite slab of thickness H which at the right end is perfectly bonded to a homogeneous elastic slab of thickness H_1.

The symmetry conditions of the problems suggest that the field variables, such as velocities, stresses, etc. depend on time t and the perpendicular distance x measured from the plane surface to which the pressure is applied.

If we denote the normal x-components of phase stresses and strains by σ_α and e_α, the

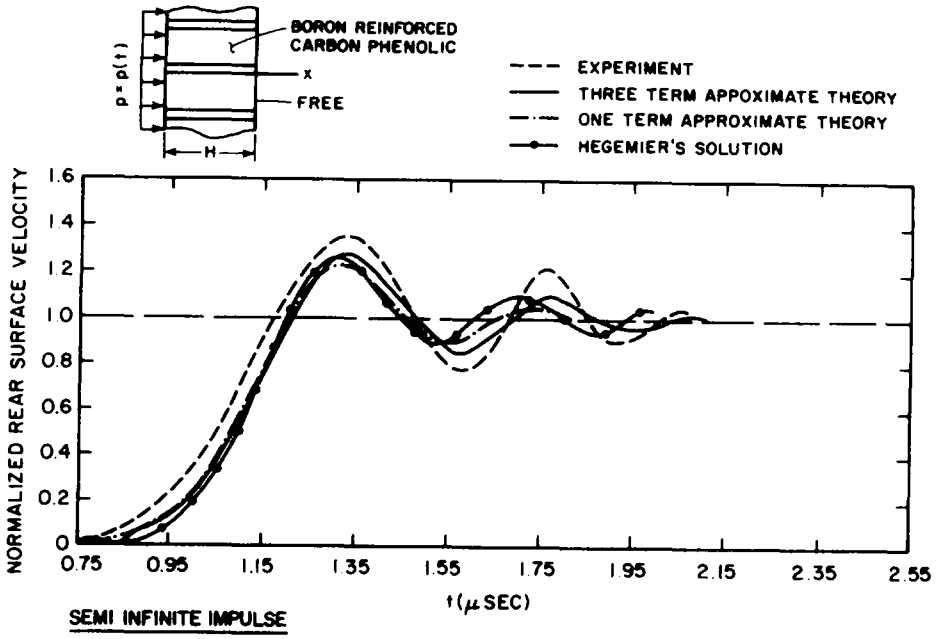

Fig. 3. Comparison of experimental and theoretical wave profiles for dilatational waves propagating parallel to layering (boron reinforced carbon phenolic laminate; semi infinite impulse).

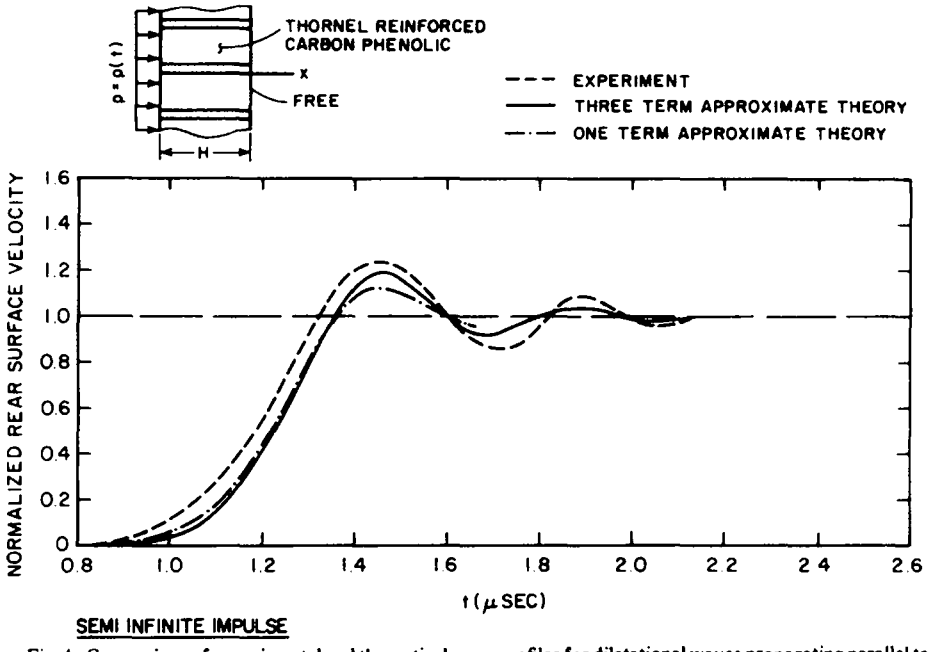

Fig. 4. Comparison of experimental and theoretical wave profiles for dilatational waves propagating parallel to layering (thornel reinforced carbon phenolic laminate; semi infinite impulse).

constitutive equations (2.5), become

$$\sigma_1 = S_{11}e_1 + S_{12}e_2$$
$$\sigma_2 = S_{12}e_1 + S_{22}e_2, \tag{3.1}$$

where

$$S_{\alpha\beta} = C_{11}^{\alpha\beta}, \text{ for propagation parallel to layering}$$
$$S_{\alpha\beta} = C_{22}^{\alpha\beta}, \text{ for propagation perpendicular to layering.} \tag{3.2}$$

Then, using eqn (2.7) the strains, e_α, are related to the x-components of the phase displace-

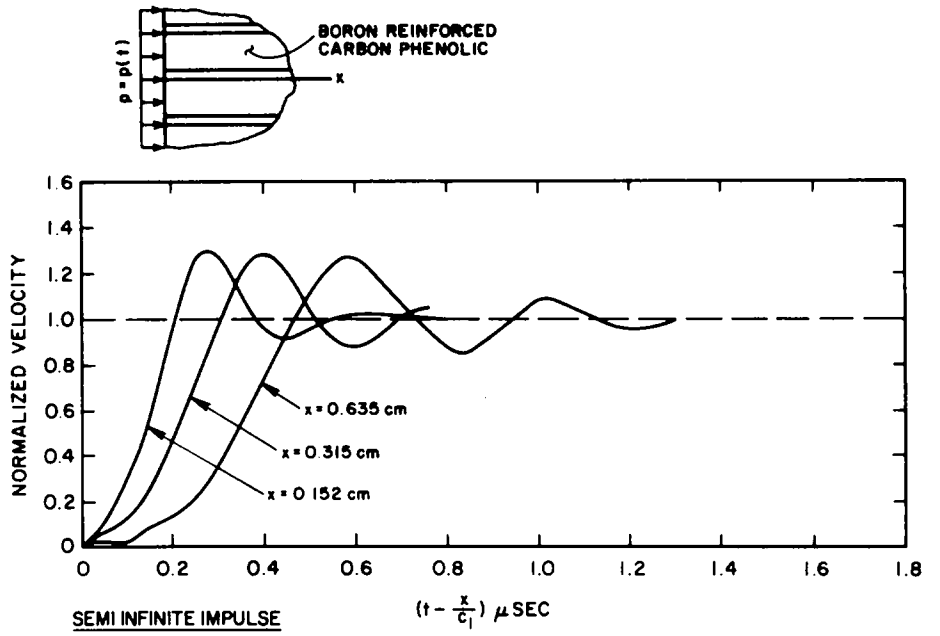

Fig. 5. Comparison of wave profiles at various stations for dilatational waves propagating parallel to layering (boron reinforced carbon phenolic laminate; semi infinite impulse).

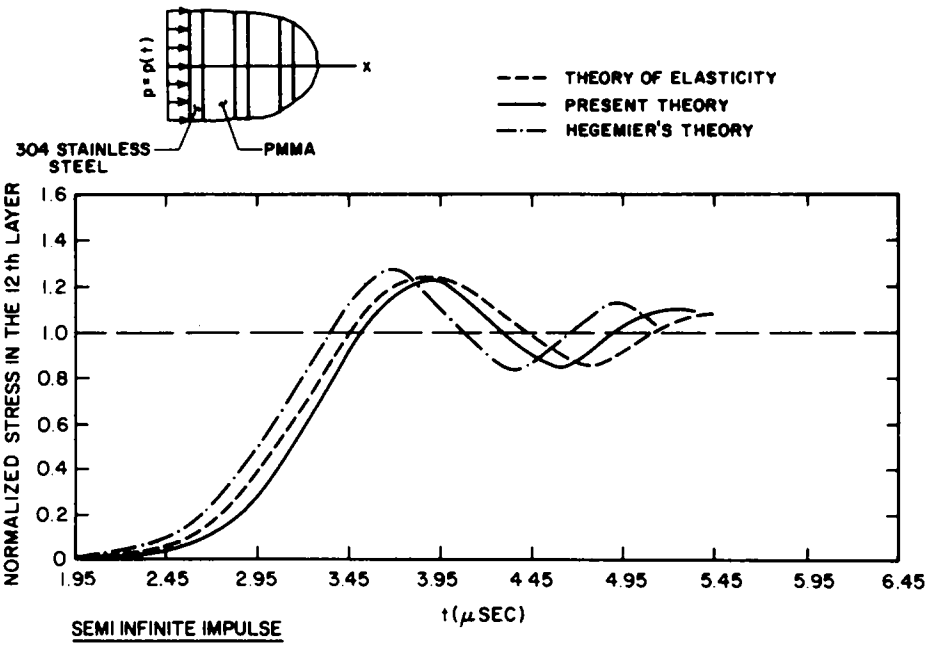

Fig. 6. Comparison of wave profiles predicted by the present theory and other theories for dilatational waves propagating perpendicular to layering (stainless steel–PMMA composite; semi infinite impulse).

ments, u_α, by

$$e_\alpha = \frac{\partial u_\alpha}{\partial x}. \tag{3.3}$$

When the weight of the composite material is neglected the equations of linear momentum (2.1) become

$$\begin{aligned} \frac{\partial \sigma_1}{\partial x} + K(u_2 - u_1) &= m_1 \dot{v}_1 - q\dot{v}_2 \\ \frac{\partial \sigma_2}{\partial x} + K(u_1 - u_2) &= -q\dot{v}_1 + m_2 \dot{v}_2, \end{aligned} \tag{3.4}$$

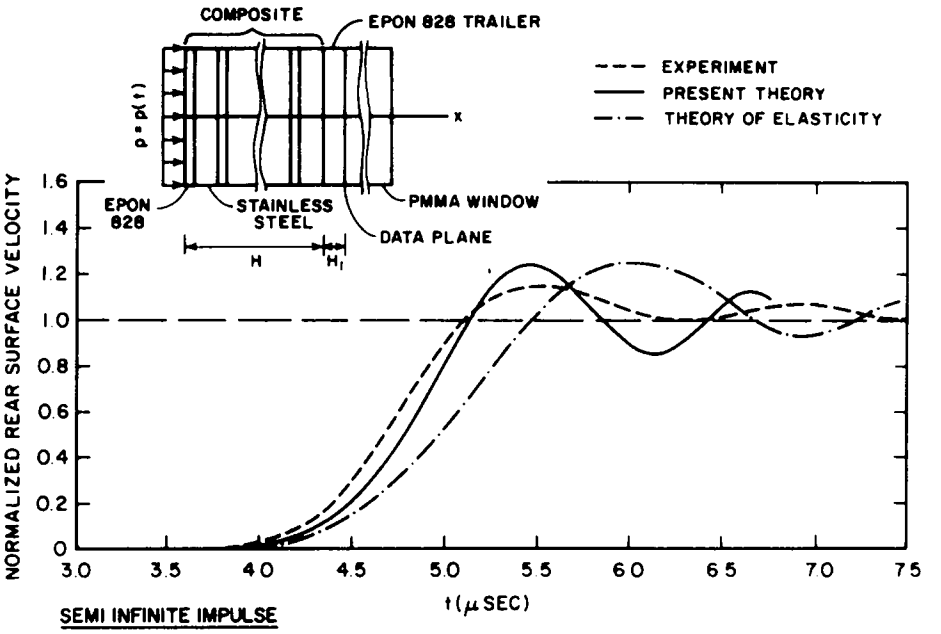

Fig. 7. Comparison of experimental and theoretical wave profiles for dilatational waves propagating perpendicular to layering (stainless steel–epon 828 composite; semi infinite impulse).

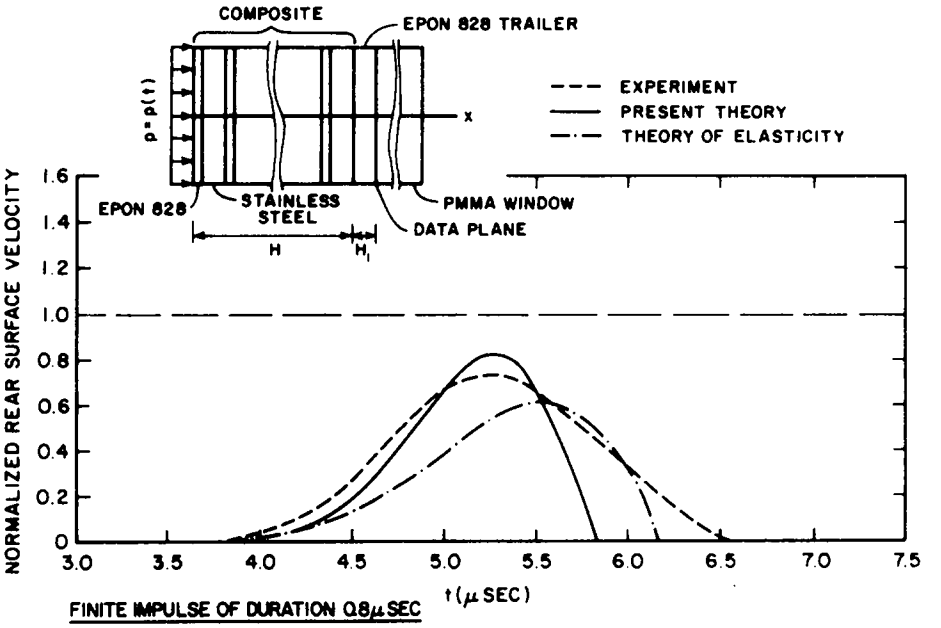

Fig. 8. Comparison of experimental and theoretical wave profiles for dilatational waves propagating perpendicular to layering (stainless steel–epon 828 composite; finite impulse of duration 0.8 μsec).

where

$$m_1 = \rho_1 + q; \qquad m_2 = \rho_2 + q \tag{3.5}$$

and

$$\begin{aligned} &K = K_1;\ q = q_1, \text{ for propagation parallel to layering} \\ &K = K_2;\ q = q_2, \text{ for propagation perpendicular to layering,} \end{aligned} \tag{3.6}$$

and v_α are the x-components of phase velocity and are related to the displacements by $v_\alpha = \dot{u}_\alpha$.

Since the medium is initially at rest all the field variables (u_α, v_α, etc.) are zero at $t = 0$.

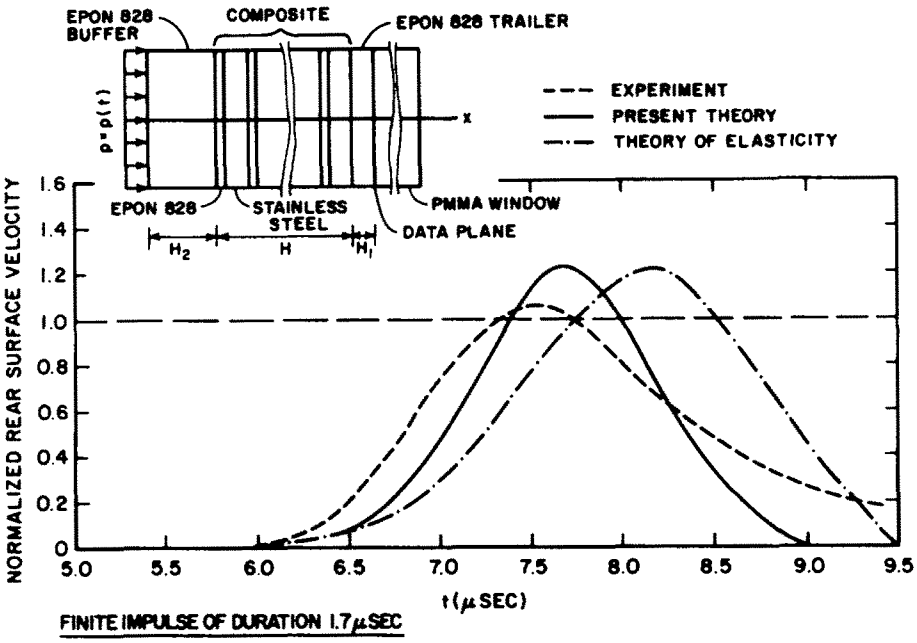

Fig. 9. Comparison of experimental and theoretical wave profiles for dilatational waves propagating perpendicular to layering (stainless steel–epon 828 composite; finite impulse of duration 1.7 μsec).

Equations (3.1), (3.3) and (3.4) constitute the governing equations of our problems. Their solutions for appropriate initial and boundary conditions, which will be discussed later, determine the time variations of the field variables (u_α, v_α, σ_α, e_α) at an arbitrary station.

4. SOLUTIONS OF THE PROBLEMS

The method of characteristics is used because the governing equations are hyperbolic and our problems contain only one space variable; furthermore this method accommodates a variety of boundary conditions.

A full discussion of the method of characteristics is given in [6]. The method of characteristics reduces the governing partial differential equations to an equivalent system of ordinary differential equations, called canonical equations, which are valid along characteristic lines only. The canonical equations are more appropriate for numerical analysis as their solutions are simple to obtain. The method of characteristics also employs decay equations from which the discontinuities across wave fronts can be computed before starting the numerical analysis.

Because of the particular types of time variations chosen for the applied pressure in the numerical analysis, which will be discussed later, the decay equations are not needed in this study. Accordingly, we present the canonical equations only.

Canonical equations

In order to put the governing partial differential equations (3.1), (3.3) and (3.4), into the form of a system of first order differential equations, we first differentiate eqn (3.3) with respect to time and obtain the compatibility equations

$$\dot{e}_\alpha = \frac{\partial v_\alpha}{\partial x}. \tag{4.1}$$

Differentiating eqn (3.1) with respect to time and using eqn (4.1) we get

$$\begin{aligned} \dot{\sigma}_1 &= S_{11}\frac{\partial v_1}{\partial x} + S_{12}\frac{\partial v_2}{\partial x} \\ \dot{\sigma}_2 &= S_{12}\frac{\partial v_2}{\partial x} + S_{22}\frac{\partial v_2}{\partial x}. \end{aligned} \tag{4.2}$$

Equations (3.4) and (4.2) constitute a system of first order differential equations. In matrix form the system has the form:

$$\mathbf{A}\bar{\mathbf{u}}_{,t} + \mathbf{B}\bar{\mathbf{u}}_{,x} + \mathbf{C} = \mathbf{0}, \tag{4.3}$$

where

$$\mathbf{A} = \begin{bmatrix} m_1 & -q & 0 & 0 \\ -q & m_2 & 0 & 0 \\ 0 & 0 & 1 & 0 \\ 0 & 0 & 0 & 1 \end{bmatrix}; \quad \mathbf{B} = \begin{bmatrix} 0 & 0 & -1 & 0 \\ 0 & 0 & 0 & -1 \\ -S_{11} & -S_{12} & 0 & 0 \\ -S_{12} & -S_{22} & 0 & 0 \end{bmatrix}; \quad \mathbf{C} = \begin{bmatrix} -K(u_2 - u_1) \\ K(u_2 - u_1) \\ 0 \\ 0 \end{bmatrix} \tag{4.4}$$

$\bar{\mathbf{u}}$ is the unknown vector defined by

$$\bar{\mathbf{u}} = \{v_1\ v_2\ \sigma_1\ \sigma_2\}^T, \tag{4.5}$$

and

$$\bar{\mathbf{u}}_{,t} = \frac{\partial \bar{\mathbf{u}}}{\partial t}; \qquad \bar{\mathbf{u}}_{,x} = \frac{\partial \bar{\mathbf{u}}}{\partial x},$$

and T denotes the transpose of a matrix or vector.

We next find the characteristic lines along which the canonical equations are valid. They are governed by the characteristic equation

$$\det(\mathbf{B} - V\mathbf{A}) = 0, \tag{4.6}$$

where $V = (\mathrm{d}x/\mathrm{d}t)$ is the wave propagation velocity. The canonical equations are then

$$\mathbf{l}^{(i)T}\mathbf{A}\frac{\mathrm{d}\bar{\mathbf{u}}}{\mathrm{d}t} + \mathbf{l}^{(i)T}\mathbf{C} = 0, \text{ valid along } \frac{\mathrm{d}x}{\mathrm{d}t} = V^{(i)}\ (i = 1\text{–}4), \tag{4.7}$$

where $(\mathrm{d}/\mathrm{d}t)$ indicates differentiation along the characteristic line with respect to time, and $\mathbf{l}^{(i)}$ is the left-hand eigen vector satisfying the equation

$$\mathbf{B}^T\mathbf{l}^{(i)} = V^{(i)}\mathbf{A}^T\mathbf{l}^{(i)}, \text{ no summation over } i\ (i = 1\text{–}4). \tag{4.8}$$

In eqns (4.7) and (4.8) $V^{(i)}$ is the ith eigenvalue determined by eqn (4.6). For our problems the four eigenvalues are

$$V^{(1)} = \sqrt{(z_1)} = C_1; \qquad V^{(2)} = -\sqrt{(z_1)} = -C_1; \qquad V^{(3)} = \sqrt{(z_2)} = C_2;\ V^{(4)} = -\sqrt{(z_2)} = -C_2, \tag{4.9}$$

where z_1 and z_2 are the roots of

$$(m_1m_2 - q^2)z^2 - [m_2S_{11} + m_1S_{22} + 2qS_{12}]z + S_{11}S_{22} - S_{12}^2 = 0. \tag{4.10}$$

Examination of eqn (3.5) will show that the coefficient $(m_1m_2 - q^2)$ is positive as $q \geqslant 0$; in addition since the strain energy function is positive definite it follows that z_1 and z_2 are nonnegative. This ensures that the $V^{(i)}(i = 1\text{–}4)$ are real. In the discussions which follow we assume, without loss of generality, that $z_1 > z_2$.

We study separately the cases for waves travelling parallel and perpendicular to layering and ascertain the appropriate wave velocities for each case by studying eqns (2.10), (2.11), (3.2) and (4.10). For the case of waves propagating parallel to layering, $(\mathrm{d}x/\mathrm{d}t) = V^{(i)}\ (i = 1, 2)$ describe two characteristic families of straight lines with slopes (C_1) and $(-C_1)$ on the $(x - t)$ plane; i.e. $x \pm C_1t = \text{const.}$ (see Fig. 1). For the same case $(\mathrm{d}x/\mathrm{d}t) = V^{(i)}\ (i = 3, 4)$ describe

another two families of straight lines $x \pm C_2 t = \text{const.}$ For the case of waves propagating perpendicular to layering the first two characteristic families are again governed by $x \pm C_1 t = \text{const.}$ (see Fig. 2). The remaining two become vertical lines parallel to the t axis because for this case $C_2 = 0$.

Finally, the canonical equations are obtained from eqns (4.3), (4.4) and (4.7). For waves propagating parallel to layering they are

$$(m_1 + qV^{(i)}a^{(i)})\frac{dv_1}{dt} - (q + m_2 V^{(i)}a^{(i)})\frac{dv_2}{dt} - \frac{1}{V^{(i)}}\frac{d\sigma_1}{dt} + a^{(i)}\frac{d\sigma_2}{dt}$$
$$- (1 + V^{(i)}a^{(i)})K(u_2 - u_1) = 0, \text{ along } \frac{dx}{dt} = V^{(i)} \ (i = 1\text{–}4; \text{ no summation on } i) \tag{4.11}$$

where the coefficients $a^{(i)}$ $(i = 1\text{–}4)$ are defined by

$$a^{(i)} = \frac{\frac{S_{11}}{V^{(i)}} - m_1 V^{(i)}}{S_{12} + q(V^{(i)})^2} = \frac{\frac{S_{12}}{V^{(i)}} + qV^{(i)}}{S_{22} - m_2(V^{(i)})^2}. \tag{4.12}$$

For waves propagating perpendicular to layering the first two canonical equations valid along the characteristic lines $x \pm C_1 t = \text{const.}$ are again given by eqn (4.11) with $i = 1$ and 2. The remaining two, which are valid along the vertical lines, are

$$\left(m_1 + \frac{S_{11}}{S_{12}}q\right)\frac{dv_1}{dt} - \left(q + \frac{S_{11}}{S_{12}}m_2\right)\frac{dv_2}{dt} - K\left(1 + \frac{S_{11}}{S_{12}}\right)(u_2 - u_1) = 0, \text{ along } \frac{dx}{dt} = 0$$
$$-\frac{d\sigma_1}{dt} + \frac{S_{11}}{S_{12}}\frac{d\sigma_2}{dt} = 0, \text{ along } \frac{dx}{dt} = 0. \tag{4.13}$$

5. NUMERICAL ANALYSIS

The purpose of this paper is to appraise the ability of the model theory to predict dynamic responses to transient inputs; therefore, the specific problems that we solve are those for which there are experimental data. These consist of four separate problems. Two involve plates of finite thickness, one having the layers parallel to the surfaces and the other perpendicular. The other two problems study the responses in half spaces, again with the two distinguished by whether the layering is parallel or normal to the surface.

The first problem involves a composite slab of thickness H subjected to a uniform dynamic pressure on one surface (see Fig. 3 or 4). The other surface is free of traction. The surfaces of the slab are perpendicular to layering so that the pressure applied generates dilatational waves that propagate parallel to the layers. We seek the solution $(\bar{u}_i) = (u_\alpha, v_\alpha, \sigma_\alpha)$ at a station x and time t. The method of characteristics is best understood by examining Fig. 1 showing the $(x\text{-}t)$ plane. On this plane the solution region is bounded by the vertical lines $x = 0$ and $x = H$. The portion of the first wave front before reflection is the line S_1 given by $x - C_1 t = 0$. This line divides the solution region into the undisturbed and disturbed regions D_1 and D_2, respectively. The reflected wave fronts are not shown in the figure because they are not needed in the numerical analysis since the time variation chosen for the applied pressure eliminates first order discontinuities across such wave fronts. To find the numerical solution, the disturbed region D_2 is subdivided by means of one primary and one secondary grid. The primary grid is shown by solid lines and formed by two sets of parallel lines $x \pm C_1 t = \text{const.}$ so that the space mesh size Δx is related to the time mesh size Δt by $\Delta x = C_1 \Delta t$. The secondary sets of grid lines are members of the families $x \pm C_2 t = \text{const.}$ and are shown by dotted lines in Fig. 1. These lines are used when analyzing an individual element. Although we note that the values of $\bar{u}_i$ along S_1 can be determined from decay equations, they are all zero here because the composite slab is initially at rest, and because the applied pressure distribution in our problems has no discontinuity at $t = 0$. To establish the $\bar{u}_i$ at points of region D_2 we start from the origin and move along S_1 where the $\bar{u}_i$ are known. Using a technique for each element, we advance into the

region, element by element, in the order $(0', 1', 2', \ldots, 0'', 1'', 2'', \ldots)$. The technique depends on the element which can be one of three types on the $(x\text{-}t)$ plane, namely, M, L and N (see Fig. 1). For an interior element M we know $\bar{u}_i$ at the points A_1, A_2 and A_5, and wish to determine it at the point A. As $\bar{u}_i$ has six components, we need six equations to establish them. Four equations come from the canonical equations (4.11), written along the lines $AA_i (i = 1\text{–}4)$. The remaining two are the compatibility equations,

$$v_\alpha = \dot{u}_\alpha, \tag{5.1}$$

which relate phase displacements to phase velocities and are valid along the vertical line AA_5. For the values of the $\bar{u}_i$ at the interior points A_3 and A_4 we use linear interpolation between the points A_1 and A_5 or A_2 and A_5. The $\bar{u}_i$ at the point A are found by integrating the six equations using an implicit trapezoidal integration formula.

For the element L, adjacent to the line $x = 0$, the procedure is the same except that the two equations along the lines AA_1 and AA_3 are replaced by the boundary conditions at $x = 0$,

$$\sigma_\alpha(A) = -n_\alpha p(A), \tag{5.2}$$

where p is the applied dynamic pressure. Similarly, for the other boundary element N the free traction boundary conditions at $x = H$,

$$\sigma_\alpha(A) = 0 \tag{5.3}$$

replace the canonical equations along lines AA_2 and AA_4.

The procedure for the problem shown in Fig. 5, involving wave propagation parallel to layering in a composite half space, is the same as that discussed for a composite slab except that the element N is disregarded since H becomes infinite for a half space.

To explain the numerical procedure for the cases for which the direction of propagation is perpendicular to layering, we choose the specific problem described in Fig. 7. The problem involves a composite slab of thickness H subjected to a uniform dynamic pressure on one surface. The other surface of the composite is perfectly bonded to a trailer of thickness H_1, which is made of a homogeneous material. For reasons which will be discussed later, the other surface of the trailer is assumed to be free of traction. We refer to Fig. 2 showing the $(x\text{–}t)$ plane and distinguish between two regions on this plane. The first, bounded by the vertical lines $x = 0$ and $x = H$, is the solution domain for the composite slab, while the second bounded by the lines $x = H$ and $x = H + H_1$, is that for the homogeneous trailer. The line S_1 describing the first wave front divides the space-time domain into the undisturbed and disturbed regions D_1 and D_2. The line S_1 is composed of two line segments. The first segment OE has the slope C_1 and represents the wave front before reflection and refraction occur at the interface $x = H$. The second segment EF describes the transmitted wave front and has the slope $C = \sqrt{[(2\mu + \lambda)/\bar{\rho}]}$, where C is the dilatational wave propagation velocity in the trailer which is identified by Lamé's constants μ and λ and the mass density $\bar{\rho}$. The primary grid for the numerical analysis is formed by the characteristic lines with slope C_1 in the composite slab region and with slope C in the homogeneous slab region. For the whole solution domain we use a common time mesh size Δt which dictates two different space mesh sizes Δx and $\Delta x'$ in the composite and homogeneous regions.

The numerical procedure for this case is basically the same as that discussed for wave propagation parallel to layering. The differences occur in the individual elements, boundary conditions and interface continuity conditions. Accordingly, in what follows, we discuss only these differences. We first note that at points in the composite region the number of unknowns $(u_\alpha, v_\alpha, \sigma_\alpha)$ is six. On the other hand the unknowns in the homogeneous region are only three, the displacement u, particle velocity v and stress σ. For the interior element M of the composite region two equations come from the canonical equations along AA_1 and AA_2, eqn (4.11) and $i = 1, 2$, two from the canonical equations along AA_5, eqns (4.13), and the remaining two from the compatibility equations along AA_5, eqn (5.1). For the boundary element L of the

composite region, the canonical equation along AA_1 is replaced by the boundary condition at $x = 0$,

$$\sum_{\alpha=1}^{2} \sigma_\alpha(A) = -p(A). \tag{5.4}$$

For the interior element P of the homogeneous region we need only three equations to find the unknowns at the point A. Two of them are the canonical equations of the homogeneous slab:

$$\begin{aligned} &\frac{d\sigma}{dt} - \tilde{\rho}C\frac{dv}{dt} = 0 \text{ along } AA_1 \\ &\frac{d\sigma}{dt} + \tilde{\rho}C\frac{dv}{dt} = 0 \text{ along } AA_2. \end{aligned} \tag{5.5}$$

The last one is the compatibility equation $v = \dot{u}$ valid along the vertical line AA_5. For the boundary element S, the free traction boundary condition at $x = H + H_1$, $\sigma(A) = 0$, replaces the canonical equation along AA_2. In the analysis of the mixed interface element Q, the interface continuity conditions

$$\sum_{\alpha=1}^{2} \sigma_\alpha(A) = \sigma(A); \qquad \sum_{\alpha=1}^{2} n_\alpha v_\alpha(A) = v(A); \qquad \sum_{\alpha=1}^{2} n_\alpha u_\alpha(A) = u(A) \tag{5.6}$$

are used.

We use the same procedure for the problem, shown in Fig. 6, involving propagation perpendicular to layering in a half space, except that the width of the composite slab is infinite. Finally for the problem shown in Fig. 9 which contains a buffer slab between the applied pressure and composite, the continuity conditions between buffer and composite are taken into account in the analysis.

6. ASSESSMENT OF THE HOMOGENEOUS MODEL

We assess the homogeneous, dispersive model and the theory which governs the propagation of waves in it, by comparing the transient wave behavior in the model with all of the data we have been able to gather describing transient wave response in layered media. Primarily these data are obtained from physical experiments but we have been able to make comparisons, for some of the cases, with the responses predicted by the exact theory and with another approximate theory due to Hegemier, Gurtman and Nayfeh[7].

The first case we study is a plate of thickness H in which the layers are aligned normal to the surfaces (Figs. 3 and 4). The response is generated by a pressure, $p(t)$, applied normal to one surface so that the resulting waves propagate parallel to the layers. The opposite face is free of traction. The response measured is the average particle velocity on the free face. The experiments on these plates were performed by Whittier and Peck[3]. Two different laminates were studied, both having a thickness $H = 0.635$ cm. The first is composed of alternate layers of thornel and carbon phenolic, the second alternate layers of boron and carbon phenolic. The mechanical properties of these materials and the layer thicknesses are listed in Tables 1 and 2, along with the necessary model constants appropriate to the homogeneous model for each of the layered materials. In accordance with the information presented in[3], the time distribution of the pressure is taken in our analysis to be a quasi step function, which is zero at $t = 0$, rises linearly to a constant value during a rise time of 0.08 μsec after which it remains constant.

The numerical analysis is carried out using a mesh size of $\Delta t = 0.005$ μsec. The responses are the time variations of the average velocity $\tilde{v} = \sum_{\alpha=1}^{2} n_\alpha v_\alpha$ at $x = H$.

Some comments on the model theory are in order. In the development of the equations of linear momentum in[2] a complicated elastodynamic operator, which appears in the equations, was replaced by a power series expansion. The major theory was obtained by retaining the first

Table 1. Properties of thornel reinforced carbon phenolic

SPECIFIED LAYER PROPERTIES							
h_1	h_2	ρ_1^R	ρ_2^R	μ_1	μ_2	λ_1	λ_2
cm		$\frac{\text{dyne-}\mu\text{sec}^2}{\text{cm}^4}$		dyne/cm^2		dyne/cm^2	
0.0032	0.0279	1.47 x10^{12}	1.42 x10^{12}	0.756 x10^{12}	0.0662 x10^{12}	0.756 x10^{12}	0.114 x10^{12}

COMPUTED MODEL CONSTANTS				
K_1	q_1	C_{11}^{11}	C_{11}^{22}	C_{11}^{12}
dyne/cm^4	$\frac{\text{dyne-}\mu\text{sec}^2}{\text{cm}^4}$	dyne/cm^2	dyne/cm^2	dyne/cm^2
227.213x10^{12}	0.399x10^{12}	0.210x10^{12}	0.220x10^{12}	0.0039x10^{12}

Table 2. Properties of boron reinforced carbon phenolic

SPECIFIED LAYER PROPERTIES							
h_1	h_2	ρ_1^R	ρ_2^R	μ_1	μ_2	λ_1	λ_2
cm		$\frac{\text{dyne-}\mu\text{sec}^2}{\text{cm}^4}$		dyne/cm^2		dyne/cm^2	
0.0052	0.026	2.37 x10^{12}	1.42 x10^{12}	0.951 x10^{12}	0.0662 x10^{12}	0.806 x10^{12}	0.114 x10^{12}

COMPUTED MODEL CONSTANTS				
K_1	q_1	C_{11}^{11}	C_{11}^{22}	C_{11}^{12}
dyne/cm^4	$\frac{\text{dyne-}\mu\text{sec}^2}{\text{cm}^4}$	dyne/cm^2	dyne/cm^2	dyne/cm^2
239.387x10^{12}	0.280x10^{12}	0.410x10^{12}	0.204x10^{12}	0.0055x10^{12}

three terms of the expansion. It was indicated in [2] that a simple cruder theory could also be developed by retaining only the first term. Responses using both of these theories were found for both laminated materials and are displayed in Figs. 3 and 4. For a comparison of these responses with the experimental data, the velocity is normalized with respect to its value at $t = \infty$ and, as the absolute times in the experiments were not measured, the experimental wave profiles are translated parallel to the time axis, so that the times corresponding to the first theoretical and experimental peaks approximately coincide. We are also able to show the response in the second plate (Fig. 3) as it is predicted by the approximate theory due to Hegemier, Gurtman and Nayfeh[7]. They obtained their numerical results by using the method of finite differences and they took the dynamic input as a step velocity impulse applied to the surface $x = 0$.

A study of Figs. 3 and 4 shows that the responses predicted by the model theory, particularly the three term theory, are close to the experimental responses. Not only are the amplitudes quite accurate, but the responses are in phase with the experimental for large times following the first disturbance. The response predicted by Hegemier in Fig. 3 is quite accurate for short times but quickly falls out of phase with the experimental profile for larger times.

The next case studied is much the same as the first cases except that the body is a half space. The forcing function is the same and alternate layers of boron and carbon phenolic are perpendicular to the surface. We use the three term theory for predicting responses and instead of comparing these with other data, we use response profiles at three stations at successively larger distances from the surface to ascertain the nature of the dispersion as the wave profile

progresses into the half space. Examination of Fig. 5 shows that close to the surface the initial part of the response is steep and the periods of oscillation are small, and as the disturbances move into the material the initial slope lessens and the periods become larger—phenomena that we would expect.

For the third case, response from the model theory is compared with two responses predicted by other theories. The body is a half space and consists of alternate layers of stainless steel and PMMA parallel to the surface. The response is generated by normal pressure applied to the surface so that the waves generated propagate normal to the layers. The properties of both the stainless steel and PMMA are shown in Table 3, along with the model constants appropriate to the laminate that are needed in finding the response. The pressure $p(t)$ is normal to the surface and has a uniform step distribution in time. To eliminate the complication of having a first order discontinuity in the solution region D_2, the discontinuity in the pressure at $t = 0$ is replaced by a linear distribution that is zero at $t = 0$ and reaches a constant value at $t = 2\Delta t$. In the numerical analysis, $\Delta t = 0.03$ μsec is used.

Comparison is made with the responses predicted by the exact theory and the theory due to Hegemier and Nayfeh[5]. The response due to the exact field equations of elasticity is complicated. The lengthy computations are based on tracing out reflected and transmitted components of one-dimensional dilatational waves.

Comparison of the responses can be made by examining Fig. 6. For early times the responses from the model and exact theories match accurately and for longer times, after the arrival of the first disturbances, the amplitudes match but the responses grow out of phase.

The final study (Figs. 7–9), is devoted to a comparison of the responses predicted by the model theory with experimental data obtained by Lundergan and Drumheller[4]. Their experiments were performed on a laminated plate of thickness $H = 1.009$ cm, composed of alternate layers of stainless steel and epon 828 running parallel to the surfaces. The properties of the layers and the values of the constants appearing in the model are given in Table 4. One surface of the plate is subjected to a uniform normal pressure, and the other surface is perfectly bonded to an epon 828 trailer. The time variation of the particle velocity is measured on the outer surface (data plane) of the trailer by using an optical interferometer observed through a PMMA window attached to the trailer at the data plane (see Figs. 7–9). Since the window material has a mechanical impedance of within 3% of that of epon 828[4], the outer face of the trailer, on which the velocity is measured, is taken as being free of traction in our analysis. The elasticity solutions in the figures correspond to the solutions obtained by using the equations of elasticity and by tracing out the wave components reflected and refracted at interfaces.

The responses shown in Figs. 7–9 all arise from the same type of excitation and differ only in their durations. Figures 7–9 have infinite, 0.8 and 1.7 μsec duration, respectively. The rise or descent time of the applied pressure is taken in all cases to be $2\Delta t$, when $\Delta t = 0.0175$ μsec. The problem described in Fig. 9 differs somewhat in that there is an epon 828 buffer between the surface of the laminated plate and the applied pressure.

Table 3. Properties of stainless steel-PMMA laminated composite

SPECIFIED LAYER PROPERTIES (AFTER HEGEMIER)					
h_1	h_2	ρ_1^R	ρ_2^R	$2\mu_1+\lambda_1$	$2\mu_2+\lambda_2$
cm	cm	$\frac{\text{dyne-}\mu\text{sec}^2}{\text{cm}^4}$	$\frac{\text{dyne-}\mu\text{sec}^2}{\text{cm}^4}$	dyne/cm^2	dyne/cm^2
0.0125	0.0392	7.9×10^{12}	1.15×10^{12}	1.258×10^{12}	0.089×10^{12}

COMPUTED MODEL CONSTANTS				
K_2	q_2	C_{22}^{11}	C_{22}^{22}	C_{22}^{12}
dyne/cm^4	$\frac{\text{dyne-}\mu\text{sec}^2}{\text{cm}^4}$	dyne/cm^2	dyne/cm^2	dyne/cm^2
128.4×10^{12}	0.185×10^{12}	0.0014×10^{12}	0.0908×10^{12}	0.0110×10^{12}

Table 4. Properties of stainless steel-epon 828 laminated composite

SPECIFIED LAYER PROPERTIES (AFTER LUNDERGAN)					
h_1	h_2	ρ_1^R	ρ_2^R	$2\mu_1+\lambda_1$	$2\mu_2+\lambda_2$
cm	cm	$\frac{\text{dyne-}\mu\text{sec}^2}{\text{cm}^4}$	$\frac{\text{dyne-}\mu\text{sec}^2}{\text{cm}^4}$	dyne/cm^2	dyne/cm^2
0.0381	0.0123	7.896×10^{12}	1.26×10^{12}	1.642×10^{12}	0.0878×10^{12}

COMPUTED MODEL CONSTANTS				
K_2	q_2	C_{22}^{11}	C_{22}^{22}	C_{22}^{12}
dyne/cm^4	$\frac{\text{dyne-}\mu\text{sec}^2}{\text{cm}^4}$	dyne/cm^2	dyne/cm^2	dyne/cm^2
362.331×10^{12}	0.645×10^{12}	0.6962×10^{12}	0.0784×10^{12}	-0.2336×10^{12}

With Figs. 3–9 we have the basis for a significant assessment of the model. We felt the need for such an assessment for a number of reasons. To review the reasons, it is important to realize that what we have is a set of equations governing the dynamic behavior of a homogeneous, elastic, dispersive material which is used to replace a two phase layered laminate. This model, as do all, consists of two parts, the form of the model, or the form of the governing equations, and the set of values of the parameters that appear in the equations. Both parts need to be assessed.

In the derivation of the equations of the model we used the classical mixture theory rather than the more complicated micromorphic mixture theory. This gave rise to some uneasiness because the classical mixture theory accommodates only the symmetrical distributions of field quantities within the phases. In the same part of the derivation, the elastodynamic operator which resulted was replaced in the final theory by an approximation consisting of the first three terms of a power series expansion.

We arrived at a set of equations for finding the nineteen model constants in terms of the layer constants in an arbitrary way, by using what seemed to us to be the simplest method. In doing so we were aware that a preferable set of parameters could be found using some rational optimization method such as system identification. We also knew that with nineteen unknowns such methods would be formidable.

The most demanding assessment seemed to us to be a comparison of experimental data with transient responses predicted by the model theory for waves propagating both parallel and perpendicular to the layers. The figures show this comparison to be quite satisfactory; for the relatively simple model with the simple method of finding the parameters, the responses appear to be accurate. Further, the accuracy is not restricted to early arrival times but extends to behavior far behind the head of the pulse.

Acknowledgement—The research reported was supported both by a grant from the National Science Foundation to the University of California at Berkeley, and NATO Project No. 1446 with the Middle East Technical University in Ankara, Turkey and the University of California at Berkeley.

REFERENCES

1. H. D. McNiven and Y. Mengi, A mathematical model for the linear dynamic behavior of two phase periodic materials. *Int. J. Solids Structures* **15**, 271–280 (1979).
2. H. D. McNiven and Y. Mengi, A mixture theory for elastic laminated composites. *Int. J. Solids Structures* **15**, 281–302 (1979).
3. J. S. Whittier and J. C. Peck, Experiments on dispersive pulse propagation in laminated composites and comparison with theory. *J. Appl. Mech.* **36**, 485–490 (1969).
4. C. D. Lundergan and D. S. Drumheller, Propagation of stress waves in a laminated plate composite. *J. Appl. Phys.* **42**, 669–675 (1971).
5. G. A. Hegemier and A. H. Nayfeh, A continuum theory for wave propagation in laminated composites. *J. Appl. Mech.* **40**, 503–510 (1973).
6. R. Courant and D. Hilbert, *Methods of Mathematical Physics*, Vol. II. Interscience, New York (1966).
7. G. A. Hegemier, G. A. Gurtman and A. H. Nayfeh, A continuum mixture theory of wave propagation in laminated and fiber reinforced composites. *Int. J. Solids Structures* **9**, 395–414 (1973).